Measurement of the LOFAR-HBA beam patterns using
an unmanned aerial vehicle in the near field

Measurement of the LOFAR-HBA beam patterns using an Unmanned Aerial Vehicle in the near-field

G. Virone,[a,*] F. Paonessa,[a] L. Ciorba,[a] S. Matteoli,[a] P. Bolli,[b] S. J. Wijnholds,[c] G. Addamo[a]
[a] Consiglio Nazionale delle Ricerche (CNR), Istituto di Elettronica ed Ingegneria dell'Informazione e delle Telecomunicazioni (IEIIT), Corso Duca degli Abruzzi 24, Turin, Italy, 10129.
[b] Istituto Nazionale di Astrofisica (INAF), Osservatorio Astronomico di Arcetri, Largo Enrico Fermi 5, Florence, Italy, 50125.
[c] Netherlands Institute for Radio Astronomy (ASTRON), Oude Hoogeveensedijk 4, Dwingeloo, Netherlands,7991.

Abstract. An Unmanned Aerial Vehicle (UAV) is exploited to characterize in-situ the High Band Antennas (HBAs) of the LOw Frequency ARray (LOFAR) CS302 station located in Exloo, The Netherlands. The size of an HBA array is about 30 m. The Fraunhofer distance (a few kms) is not reachable in the frequency band (120 - 240 MHz) within the flight regulation limits. Therefore, far-field patterns cannot be directly measured. The UAV, equipped with an RF synthesizer and a dipole antenna, flies in the near-field region of the considered array. Measurement of three different frequencies (124, 150, 180 MHz) is efficiently made during the same UAV flight. The near-field focusing method is exploited to validate the far-field pattern of the array under test within an angular range around the beam axis. Such a technique avoids both the time consuming $\lambda/2$ sampling of the aperture field and the further application of computationally heavy near-field to far-field transformations. The array beam is well reconstructed in the main lobe and first sidelobes within a 2D scan plane sampled with a radial raster. A further post-processing technique is proposed and validated on a subarray of HBAs. It suggests efficient ways for the future characterization of regular aperture arrays for SKA-Mid Phase 2.

Keywords: antenna measurements, unmanned aerial vehicle, near-field focusing, VHF band, large arrays, hybrid beamforming.

***Giuseppe Virone**, E-mail: giuseppe.virone@ieiit.cnr.it

1 Introduction

The LOw Frequency ARray (LOFAR) [1] is a radio telescope composed of 52 stations located in Europe. Each station is composed of two subarrays, one with Low-Band Antennas (LBAs) and one with High-Band Antennas (HBAs). Their operating frequency range is 10 - 90 MHz and 120 - 240 MHz, respectively. LBAs are arranged in a random configuration whereas HBAs are placed in a regular lattice.

LOFAR is a pathfinder for the international Square Kilometre Array (SKA). The SKA will become the biggest and most sensitive radio telescope in the world. Aperture arrays are envisioned for both

SKA1-Low (50 - 350MHz, random configuration) [2], [3] and possibly SKA1-Mid Phase 2 (400 MHz – 1.45 GHz, regular configuration) [4], [5], [6]. Dishes will be adopted for higher frequencies up to 14 GHz.

All these powerful radio telescopes need to be validated and accurately calibrated. Of course, testing these large arrays is not an easy task due to their large size and the low operating frequencies. A few approaches have been proposed exploiting measured data in far or quasi-far field condition. For example, a holographic technique has been applied to the Engineering Development Array 2 of SKA1-LOW [7] and LOFAR [8] to retrieve aperture fields. Other tests on LOFAR have been performed using astronomical calibration sources [9] and RF sources mounted on cranes [10].

More recently, thanks to the technological development of Unmanned Aerial Vehicles (UAVs), flying test sources have been developed to test aperture arrays even at element level [11] - [16] with a high signal-to-noise ratio and a huge scan flexibility. Due to the large electrical size of the aperture arrays, the Fraunhofer distance cannot always be reached. Therefore, validation of LOFAR LBA array has been performed comparing measurement and simulation in the near field [17], [18]. All previous papers featured sparse arrays with particular emphasis on the random configuration [19]. In this work, the UAV-based measurement strategy is extended to the LOFAR HBA (Fig. 1) which is a large regular array. Near field focusing [20], [21] is adopted and its validity is assessed by comparison to the far-field simulated data (Section 2). This procedure has been applied on a two-dimensional scan path to provide a more complete characterization (Section 3). A first attempt to develop a far-field reconstruction strategy (to overcome the artifacts of the near-field focusing) and the corresponding definition of efficient near-field scan strategies for regular arrays such as the aperture arrays for SKA-Mid Phase 2 is presented in Section 4.

To summarize, the novelty aspects of this paper are:

1) The verification of all tiles within a single flight over a LOFAR-HBA substation;

2) The application of near-field focusing to an array of tiles pointed in the same far-field direction to provide an end-to-end verification of the system from the antennas to the digitized data;

3) The usage of radial raster scans to represent the beam pattern in the u-v plane with a limited set of linear scans, which is an efficient choice in view of the limited UAV flight duration compared to cartesian rasters [11];

4) The definition of a far-field reconstruction strategy to partially overcome the artifacts of the near-field focusing and its validation on a subarray of the HBA substation.

Fig. 1. The UAV after take-off is reaching the first waypoint to perform the required scan path over a LOFAR HBA array of the CS302 station. The array size is about 30 m.

1.1 UAV-mounted test source and the HBA

The UAV is visible in Fig. 1. It is equipped with a differential Global Navigation Satellite System (GNSS) receiver for accurate positioning within a few centimeters, a dipole antenna and a RF synthesizer [13]. Three higher-order harmonics of the RF synthesizer (i.e., it was operating as a comb generator) have been used during the same flight. In this way, three different frequencies (i.e., 124, 150 and 180 MHz) have been measured simultaneously. This procedure is applicable when the receiver acquisition system can simultaneously record many frequency channels to drastically reduce the flight time of the UAV.

Fig.1 also shows the Eastern HBA array of the CS302 LOFAR station located in Exloo. The detailed geometry of this LOFAR HBA subarray is shown in Fig. 2. It is composed of 24 square tiles (red numbers from 0 to 23) with a size of about 5 by 5 m^2. Each tile is composed of a regular distribution of 4 by 4 dual-polarized elements i.e. thin crossed-bowtie dipoles suspended over a ground plane by means of a polystyrene support structure. The dipole length is about 0.7 m. Within each tile, the element spacing is 1.25 m [1]. The distance between tile centers is 5.15 m, therefore, the spacing between elements of adjacent tiles is slightly larger (1.4 m) than within the tile. Nevertheless, the overall distribution can be considered as very close to a uniform regular array. Through the analog beam forming, each tile can be pointed within a field of view of 60 degrees around zenith. Furthermore, signals from all tiles can be summed together by digital beam forming.

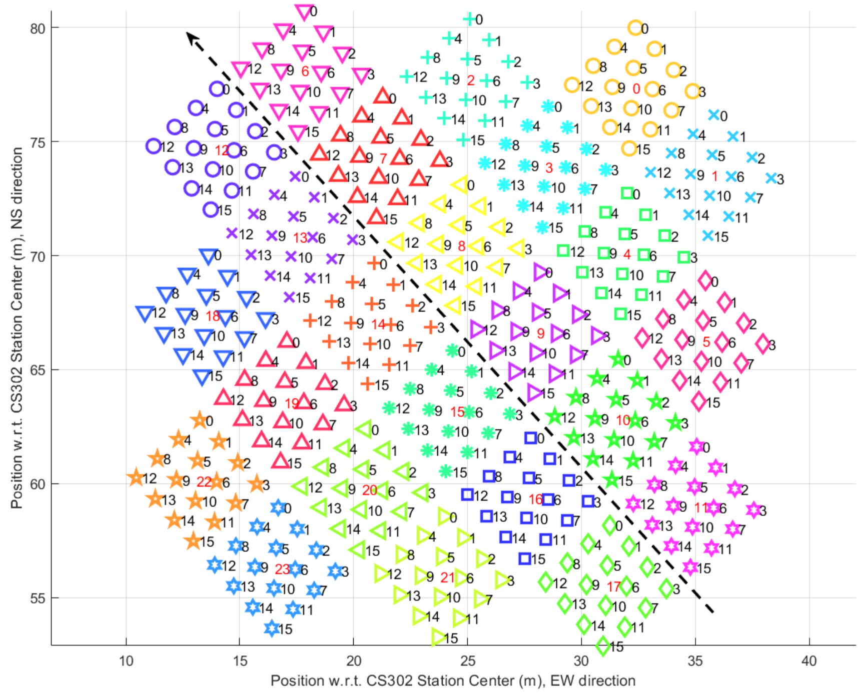

Fig. 2 Element positions in the LOFAR HBA subarray. Red and black numbers refer to tile number (0-23) and element number (0-15) inside the single tile, respectively. The black dashed curve shows an example of a UAV path (its projection to the ground) oriented along the North-West direction.

The two element polarizations are oriented along the North-West and North-East directions. For the considered CS302 station, the orientation of the regular array distribution is 48° from North (see Fig. 2). Hence, there is a 3° rotation between element polarization directions and array lattice principal directions. Nevertheless, the labels "North-West" and "North-East" will be still adopted in this paper for both polarization and array principal (periodicity) directions for the sake of simplicity.

2 Beam patterns using near-field focusing

Several flights with linear trajectories and constant height have been performed. A sketch of a UAV path projected to the ground and oriented North-West is shown in Fig. 2 with the black-dashed line. This section presents the results obtained for a flight where both the UAV speed vector and the onboard dipole are oriented North-West. This corresponds to an E-plane scan of the array elements oriented North-West. The UAV flight duration to perform this single linear path was approximately 1 minute (flight speed was about 3 m/s) whereas 2-3 minutes are necessary for take-off and landing. The flight height has been maintained at 140 m due to regulation limitations. This already satisfies the far-field condition for each tile (Fraunhofer distance is 60 m at 180 MHz) but is not enough for the full array (about 1.1 km at 180 MHz). This fact is confirmed in Fig. 3, where the measured tile beams (E-plane, 124 MHz) are shown for the tiles closest to the projection of the UAV path (dashed black line in Fig. 2), i.e., tiles 6-11 and 12-17. The effect of UAV pattern and path loss has been removed as in [22]. All beams are reported with respect to the curvilinear abscissa on the UAV path. The origin of the curvilinear abscissa is set where the UAV path projection is closest to the center of the HBA array. The analog beam formers were programmed to point the tile beams at zenith. However, because of the low altitude of the UAV, the maxima of the tile beams occur at different values of the curvilinear abscissa. In particular, the maxima of tiles 11 and 17 occur at about -13 m, whereas the maxima of tiles 6 and 12 occur at +13m. This is consistent with the distance between tile centers of about 26 m. The successful comparison with simulations at tile level was already reported in [23]. In this work, the tile beams are instead used to estimate the full array pattern by means of a near-field focusing method [20]. However, it should be mentioned that, differently from [17], the presence of analog beam-formers at tile level prevents the application of the required parabolic phase shifts across the array aperture i.e., to each array element. Such near-field focusing can only be applied on the tile signals. In other words, the tile beams are pointed to zenith (far-field) whereas the array of tiles will be focused in near-field. All the tile beams in Fig. 3 are normalized in magnitude and phase at the origin of the curvilinear abscissa to produce the near-field focusing for the array of tiles. The parabolic phase shifts for the various tiles are automatically produced by the different electrical distances with respect to the UAV-mounted source placed in the near-field.

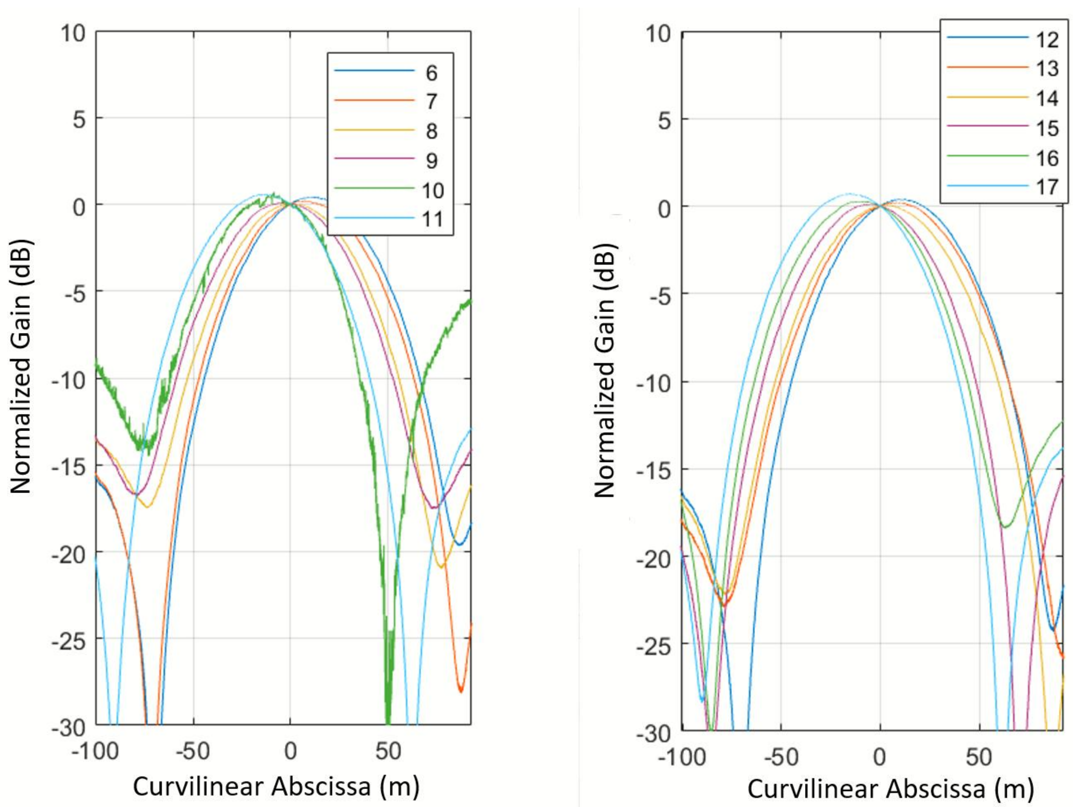

Fig. 3 Normalized E-plane radiation pattern for tiles 6-11 (left) and 12-17 (right) at 124 MHz.

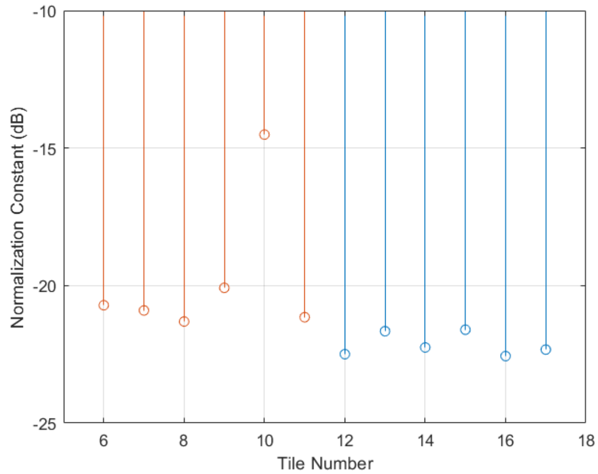

Fig. 4 Normalization constants (dB) for tiles 6-17 at 124 MHz.

Normalization constants in magnitude are shown in Fig. 4. It is apparent that tile number 10 requires a larger normalization constant with respect to the other tiles to achieve proper equalization. From Fig. 3, it can be also noted that its signal is noisier and the sidelobes are higher with respect to all the other tiles. This can be explained with a fault in the analog beam former of tile 10.

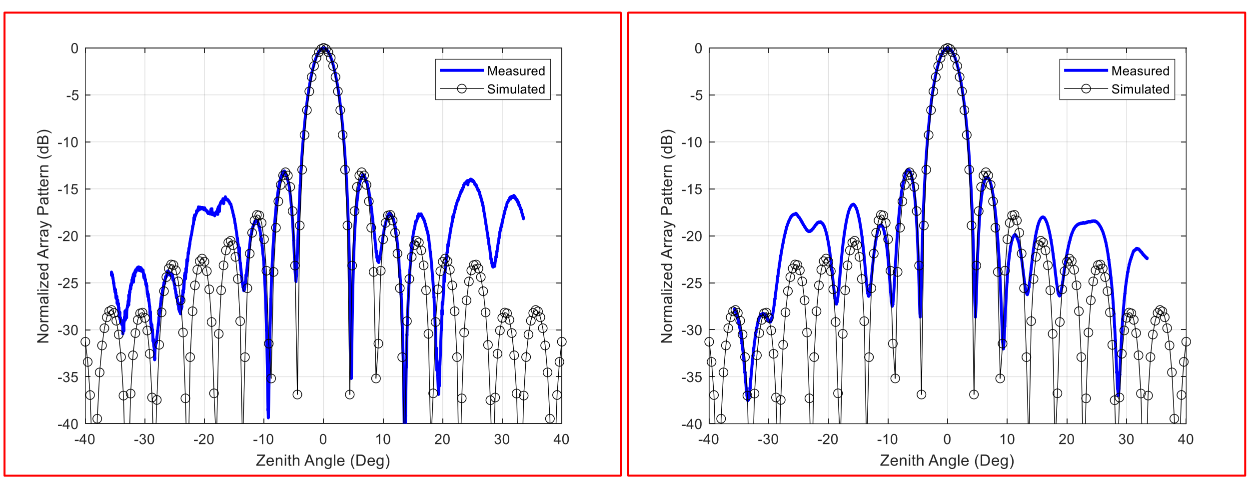

Fig. 5 Far field pattern (black line) and focused near field (blue line) of tiles 6-11 (left panel) and 12-17 (right panel) at 124 MHz.

The equalized (magnitude and phase) signals from the two tile rows 6-11 and 12-17 have been summed together to obtain the radiation patterns at 124 MHz that are shown in Fig. 5 (blue line) as a function of the zenith angle. The zenith angle has been computed using the curvilinear abscissa and the UAV height. A far-field simulation obtained using a combination of WIPL-D and array factor is also shown in Fig. 5 (black solid line with circular markers). WIPL-D has been used on a subarray of 3 by 3 tiles, i.e., 12 by 12 dipoles. This configuration requires neither significant computational effort nor specific acceleration methods. However, it allows to estimate the effect of mutual coupling on the tile beam. Differences between the nine simulated tile beams in the 3 by 3 tile array have been found to be negligible with respect to the measured discrepancies [23]. For this reason, an array factor approach has been adopted using the simulated tile beam (central tile within the 3 by 3 array) as element pattern. The agreement is satisfactory within ±15° from zenith. This is consistent with the near-field focusing method, which guarantees a good agreement between far-field and near-field focused beams only in the proximity of the beam axis [20]. The level of first sidelobes (-13 dB) is consistent with the uniform amplitude excitation. The pattern of the array of tiles 6-11 shows larger discrepancies with respect to simulation because of the faulty tile 10. Almost the same level of agreement has been obtained at 150 and 180 MHz (see Fig. 6, only the array of tiles 12-17 has been reported for brevity). As expected, the angular region with good agreement becomes narrower at higher frequencies (±10° from zenith) because the Fraunhofer condition increases with frequency and all frequencies were measured during the same flight and, hence, at the same height.

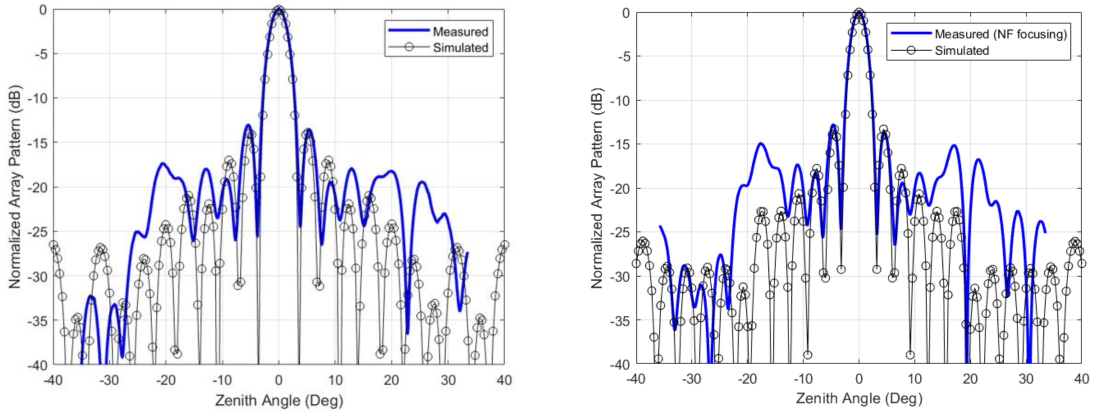

Fig. 6 Far field pattern (black line) and focused near field (blue line) of tiles 12-17 at 150 MHz (left) and 180 MHz (right).

The same near-field focusing procedure has been applied to the full HBA array in Fig. 2. No further faulty tile has been found besides number 10 (it should be noted that all the tiles in Fig. 2 have been verified in such a single flight). Figs. 7, 8 and 9 show the measured (near-field focused) and the simulated (far-field) radiation patterns at 124, 150 and 180 MHz. The angular region showing good agreement is again ranging from ±15° to ±10° at lower and higher frequencies, respectively. The Full Half Power Beamwidths are 5.2°, 3.9° and 3.4° at 124, 150 and 180 MHz, respectively. The low level of the first sidelobes is due to the array geometry. It should be noted that all the tiles in Fig. 2 contribute to the array pattern. The number of tiles along the direction that is orthogonal to the UAV scan i.e. the number of tiles along North-East direction is six in the array center and two at its edges. As far as the North-West cut reported in Figs. 7, 8 and 9 is concerned, this is equivalent (in the far-field) to a linear array with edge tapering, which in turn explains the low sidelobes. This fact can be easily demonstrated by computing the array factor along the North-West cut.

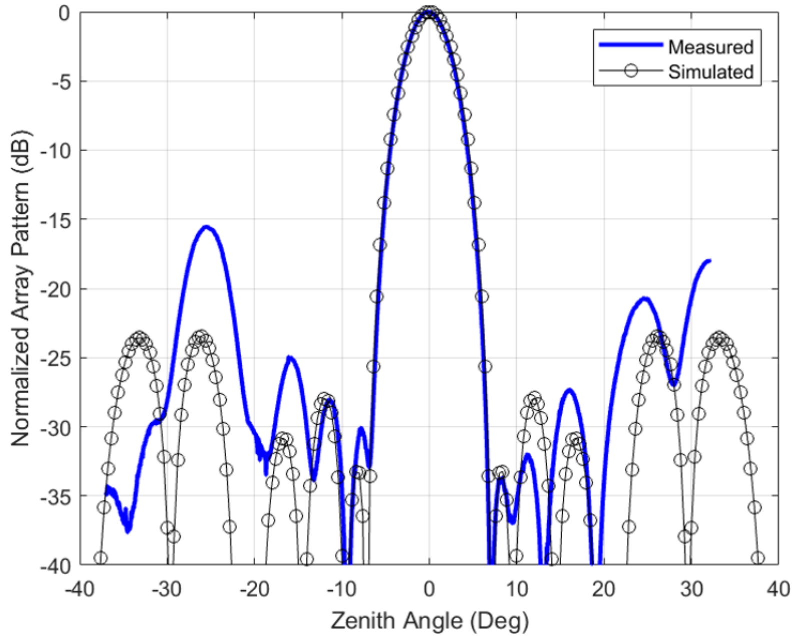

Fig. 7 Far field pattern (black line) and focused near field (blue line) of tiles 1-24 (full HBA subarray) at 124 MHz.

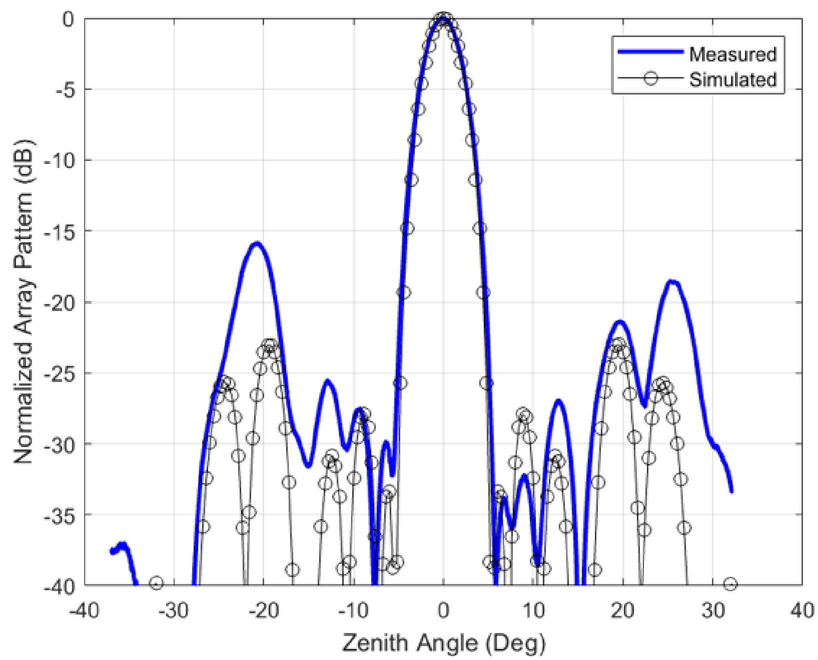

Fig. 8 Far field pattern (black line) and focused near field (blue line) of tiles 1-24 (full HBA subarray) at 150 MHz.

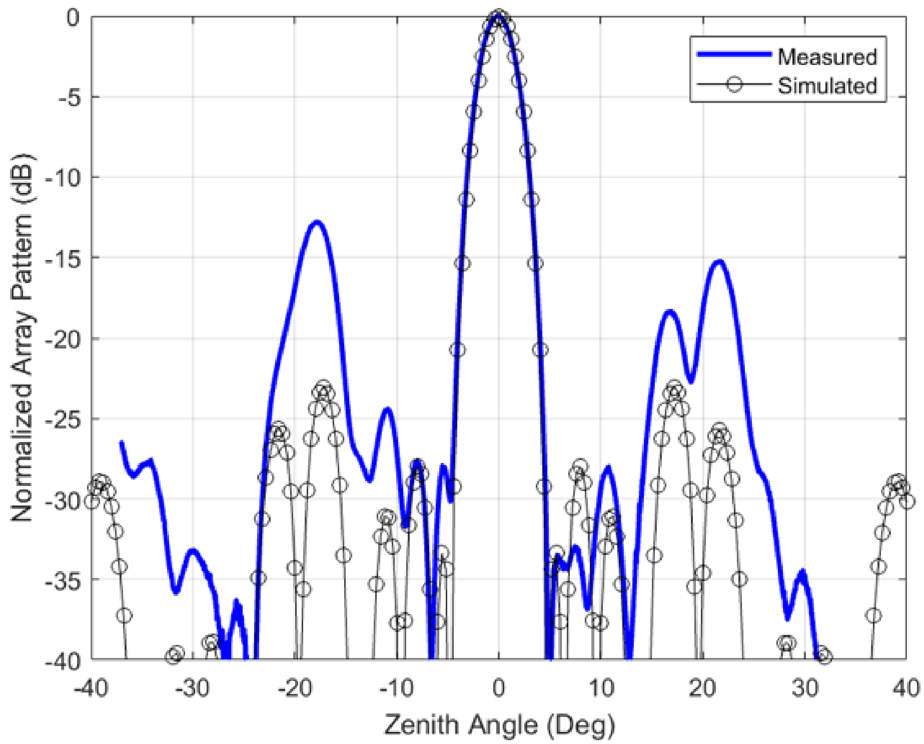

Fig. 9 Far field pattern (black line) and focused near field (blue line) of tiles 1-24 (full HBA subarray) at 180 MHz.

3 Radial Rasters as an efficient scan strategy

The results in section 2 concern a single linear scan performed along the North-West direction. Additional linear scans were performed with an angular offset of 22.5° to achieve a more complete coverage of the u-v plane (directional cosines). All angular steps were performed with two orientations of the UAV-mounted dipole i.e., parallel and orthogonal to the speed vector to sample both the θ- and φ-components of the radiation patterns. Each raster has been split as two flights for each field component i.e. a total of four flights. The duration of each flight has been approximately 10 minutes. The full flight duration capability of the UAV has not been exploited due to the severe wind condition observed during the campaign. A larger margin on the battery charge has been maintained for safety reasons. Longer flight durations up to 40 minutes are now available with modern UAVs operating in calm wind condition. The measured results for the North-West polarized elements of tile number 9 (see Fig. 2) are shown in Fig. 10.

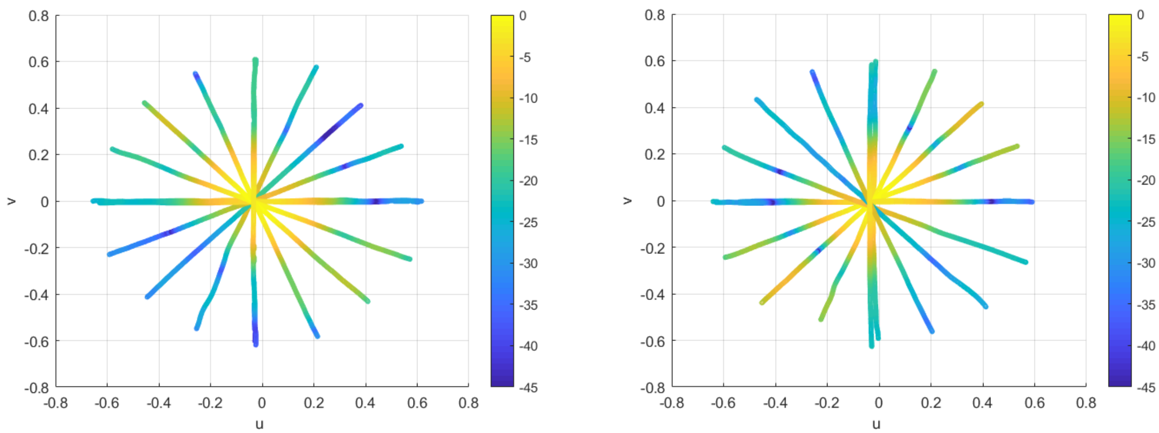

Fig. 10 Measured θ- (left) and φ- (right) components of the radiated pattern in dB of tile 9 at 180 MHz (Elements polarized along North-West, i.e. +135° from u axis).

The North-West radiation pattern cut (+135° from u axis) for the (radial) θ- component (on the left panel of Fig. 10) corresponds to the E-plane co-polar pattern for the tile elements polarized along the North-West direction (same cut that is discussed in both section 2 and [23]), where both main lobe and sidelobes are visible. The cut oriented North-East (θ- component, left side of Fig. 10) instead represents a cross-polar H-plane pattern, which is quite low in magnitude as expected. The H-plane co-polar pattern in visible in the right panel of Fig. 10 where the (azimuthal) φ-component is shown. The North-East cut shows again both main lobe and first sidelobes. This is consistent with the square geometry of the tiles.

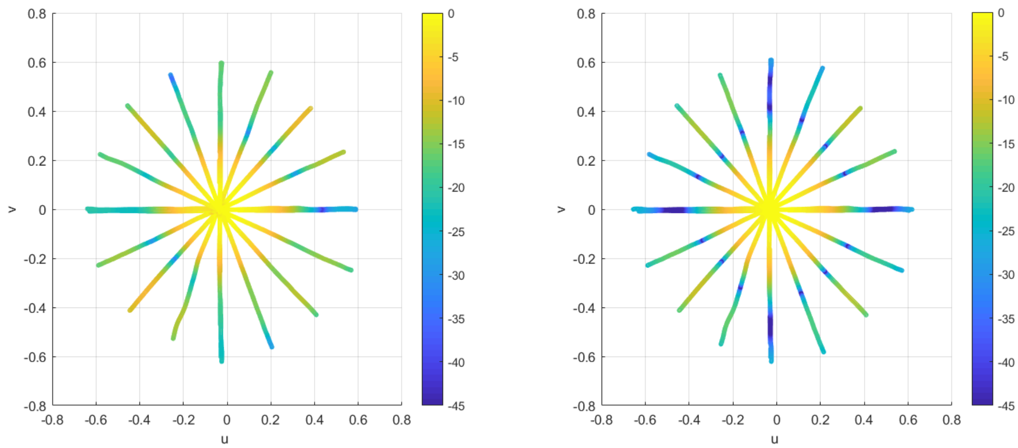

Fig. 11 Measured (left) an simulated (right) beam patterns in dB for tile 9 at 180 MHz (North-West polarized elements).

The power pattern, i.e., the combination of the two orthogonal pattern components in Fig. 10, is shown in Fig. 11 (left). Both E-plane and H-plane are now visible on the same plot as North-West and North-East paths, respectively. The symmetry of the beam, which is due to the square geometry of the tiles is clearly visible. The overall pattern is very consistent to the simulated data on the right of Fig. 11. The main difference is the depth of the nulls, which is mainly related to source orientation errors, modeling errors and of course manufacturing and position uncertainties of the real tile. Manufacturing tolerances are neither calibrated nor corrected for in the analog beamformer.

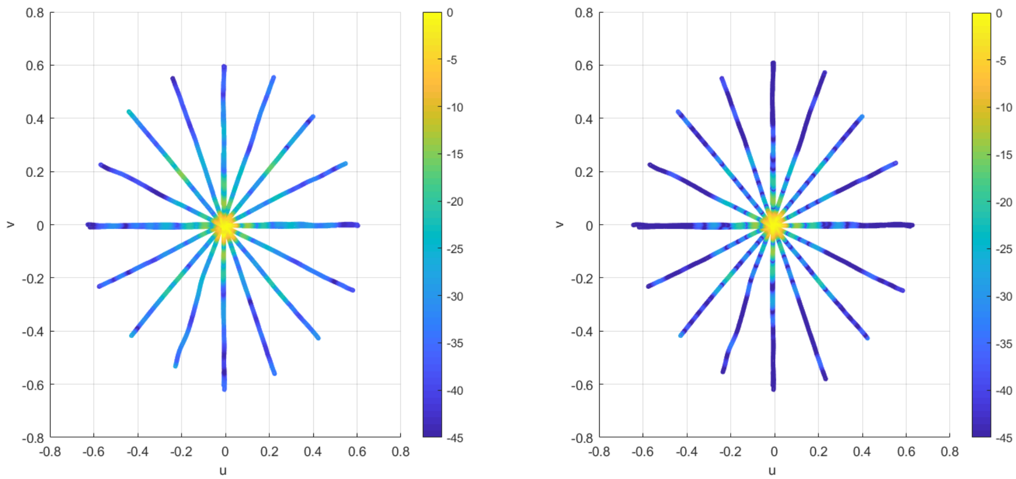

Fig. 12 Measured (left) and simulated (right) beam patterns in dB of the HBA array in Fig. 2 at 180 MHz (North-West polarized elements).

The near-field focusing method described in section 2 has been applied to the full HBA shown in Fig. 2. The result is shown in Fig. 12 (left side) and is in good agreement with the simulation (right side). The beam symmetry and width are consistent. Artifacts are still visible in both the North-West and North-East paths. Nevertheless, these results provide a good in-situ validation of the HBA substation.

For brevity, we have only presented results for the HBA elements polarized along the North-West direction. However, similar results have been achieved for the North-East ones.

4 Far-field reconstruction

This section presents an alternative strategy to partially overcome the artifacts due to near-field focusing method already discussed in section 2. It is based on the consideration that the performed UAV flights satisfy the far-field condition for the tiles but not for the array of tiles. For the tiles, both amplitude and phase of the acquired signals are available (complex voltages). The amplitude patterns can be easily obtained by geometrical considerations i.e. the amplitude data for each tile (after removal of UAV pattern and path loss, see for example Fig. 3) are expressed as a function of a local reference system centered on the tile itself, instead of the center of the full array. The resulting patterns for tiles 12-17 are shown in Fig. 13. The frequency of 180 MHz has been selected for this example because it represents a worst case for the near-field focusing artifacts.

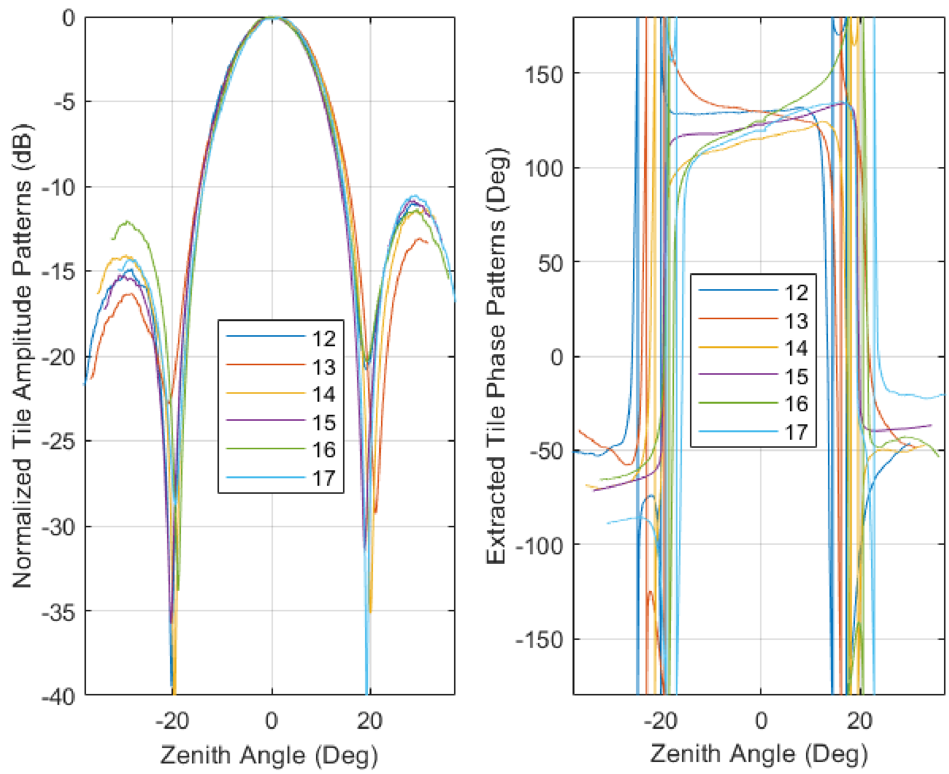

Fig. 13 Reconstructed far-field E-plane radiation patterns for tiles 12-17 at 180 MHz: magnitude (left) and phase (right). Near field plots are instead shown in Fig. 3.

As far as far-field phase patterns are concerned, their determination is less straightforward because the UAV-mounted RF source is not phase-locked to the on-ground acquisition system of the telescope. In other words, the relative phase between transmitter and receivers is drifting during the flight in an uncontrolled way. For this reason, only differential phase data can be used [24]. In [25], a reference antenna with known phase pattern was placed in the proximity of the SKA-LOW array prototype to reconstruct a near-field phase pattern. In this campaign, no reference antenna was available. Therefore, one of the central tiles (i.e., tile number 15) is used as reference. This, of course, relies on the knowledge of its phase pattern by simulations (see Fig. 13, right side, violet curve). Under this hypothesis, the phase patterns of all other tiles $\emptyset_j$ can be computed as

$$\emptyset_j=\emptyset_i+\varphi_j-\varphi_i+k(r_j-r_i) \tag{1}$$

where the time/position dependence of all the terms has been understood, $\emptyset_i$ is the phase pattern of the reference tile (i =15 in our case), φ_j and φ_i are the phase of the acquired complex voltages, k is the wave number and r_j, r_i are the distances between the UAV-mounted source and the centers of tiles j and i, respectively. It should be mentioned that in (1), the direction dependence of the source pattern has been neglected (it is in the order of a few degrees). Moreover, only the co-polar component is considered (transmitter and receiver are matched in polarization). The relative distances r_j and r_i are computed exploiting the UAV position data measured by GNSS and the knowledge of the tile center positions (nominal data have been used, however, an accurate measurement with ground-based instruments such as total station or GNSS is viable). The resulting reconstructed far-field phase patterns for tiles 12-14 and 16-17 are shown on the right side of Fig. 13. They are quite similar to each other because local reference systems (centered on each tile) have been adopted. Each of them shows narrow anomalies where the phase rotates of 360° around the zenith angle ± 20°. These anomalies are due to the two nulls on the pattern of the reference tile. At the nulls, the phase exhibits abrupt variations of 180°. In these regions, the accuracy of the models is generally lower and therefore, a perfect cancellation between the terms $\emptyset_i$ and φ_i does not occur in (1). A reference antenna with a smoother behaviour would be desirable to avoid such anomalies (this can be implemented by either activating only one dipole within a tile that will be hence used as reference only or exploiting an additional external reference antenna in the proximity of the HBA). Nevertheless, after summation of the tile patterns in Fig. 13, the resulting beam in Fig. 14 (red curve) is more consistent to the far-field simulation (black curve) than the previous near-field focusing data (blue curve). It should be mentioned that, before summation, the tile phase patterns in Fig. 13 have been both converted to the same reference system by exploiting again the knowledge of the tile center positions and equalized at zenith (array calibration). The angular regions where the discrepancies occur are consistent with the position of the reconstructed far-field phase pattern anomalies in Fig. 13. A better agreement has been also achieved at 124 MHz (see Fig. 15) using the same reconstruction method. The overall improvement has been quantified computing the average (along zenith angle) of the weighted logarithmic difference $\Delta_{w,log}$ in [26] with β=0.5 between measurements and simulation. For the near-field focusing (blue curve), the quantity $\Delta_{w,log}$ is 0.89 dB and 1.15 dB at 124 and 180 MHz, respectively. A smaller $\Delta_{w,log}$ of 0.68 dB has been achieved for the reconstructed far-field case (red curve) at both frequencies.

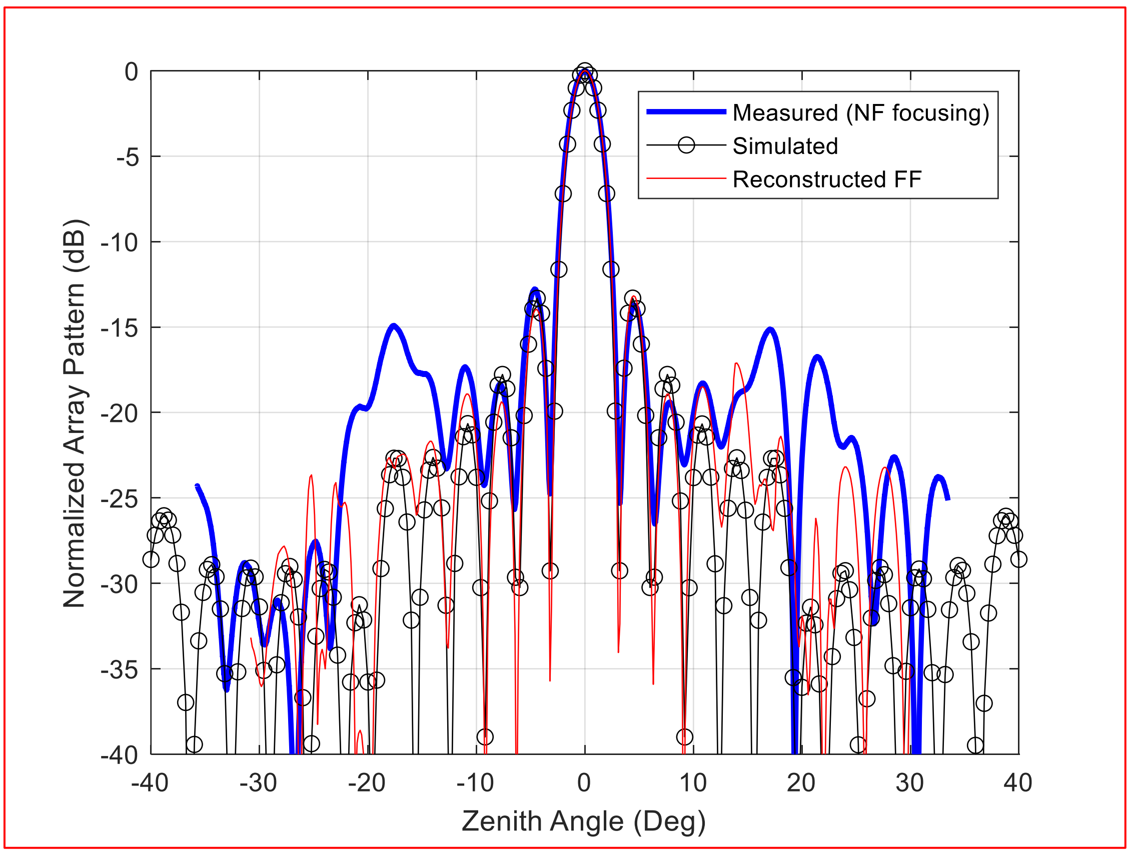

Fig. 14. E-plane radiation pattern for the subarray of tiles 12-17 at 180 MHz.

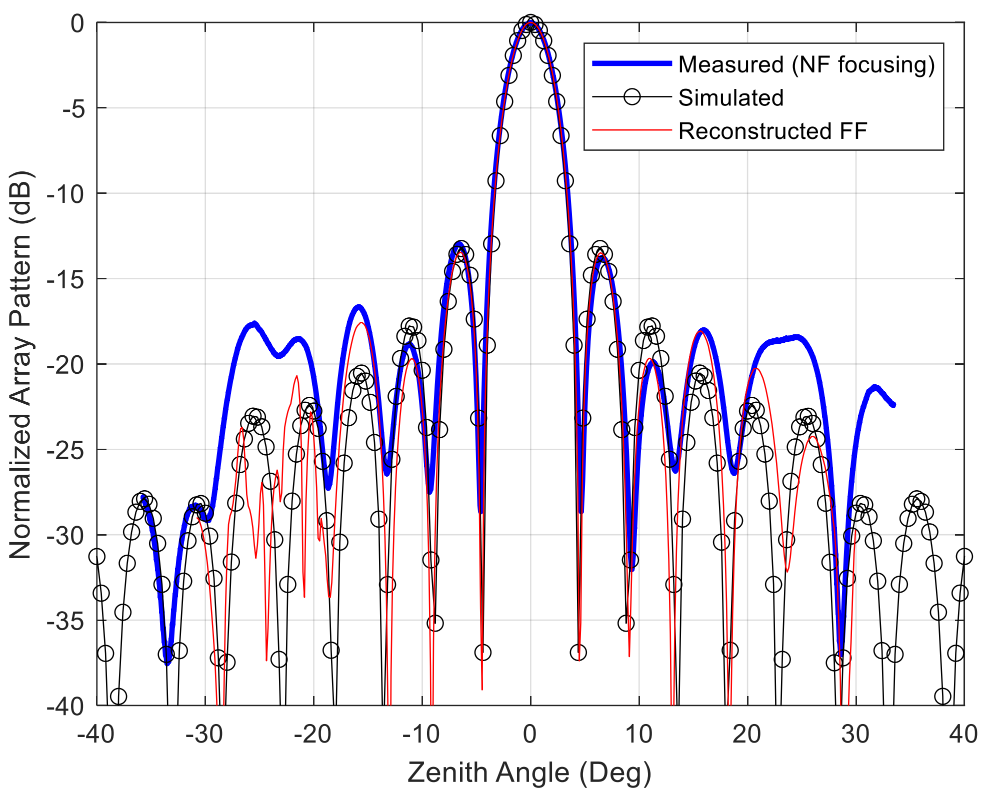

Fig. 15. E-plane radiation pattern for the subarray of tiles 12-17 at 124 MHz.

The method presented in this section has only been applied to the linear array of tiles 12-17 which is close to the North-West scan path performed by the UAV (see Fig. 2). The array of tiles 6-11 has not been considered because of the faulty tile. The best condition for the presented far-field reconstruction is a scan path that intersects the maxima of the tile beams, whose pointing is set before the flight. Otherwise, the information of the principal cut of the tile radiation pattern is not available. A linear flight parallel to the array lattice direction (almost North-West in this case) will intersect the maximum number of tile beam maxima. According to these considerations, a cartesian raster with 6 x 6 orthogonal linear scans and a spacing of 5.15 m (distance between tile centers) would have allowed the measurements of all the tile patterns in their principal planes and the subsequent reconstruction of the full array far-field pattern along the North-West and North-East planes by using the method presented in this section. It should be noted that a raster that is suitable for a near-field to far-field transformation would have required a spacing of less than λ/2 i.e., 0.8 m at 180 MHz, with a strong impact on the UAV flight time requirement. Moreover, a computationally heavy inversion algorithm must be applied [27] to transform the scan paths performed by UAV in the near-field. The presented solution, together with the exploitation of a smoother and well-known reference antenna could be considered for the characterization of the regular arrays of SKA-mid.

5 Conclusion and future developments

The application of near-field focusing to an array of LOFAR-HBA tiles pointed in the same far-field direction demonstrated that a useful end-to-end system validation can be performed even considering only a limited angular range around the beam axis. Simulated and measured results are in good agreement as far as beamwidth and first sidelobes are concerned. The method also pointed out the presence of a faulty tile in the Eastern HBA subarray of the CS302 station.

The combination of a few linear scans with different orientations has been performed to achieve a radial raster. This procedure confirmed the agreement between measurements and simulations on the full u-v plane, although with limited coverage. The angular step of 22.5° could be reduced at the expense of a longer flight/scan duration.

A far-field reconstruction method has been proposed and validated on a linear subarray of the HBA substation. It allows to partially overcome the artifacts of the near-field focusing strategy exploiting the usage of a known reference antenna and the knowledge of the tile positions. This suggests a validation procedure for regular aperture arrays such as SKA-mid that is based on a cartesian raster in the near-field with a spacing that is equal to the tile spacing, which is several times larger than λ/2. This efficient scan strategy will provide far-field pattern information on the principal planes only, which could already be satisfactory as far as validating stations in-situ is concerned.

Acknowledgments

The authors would like to acknowledge M. J. Norden from ASTRON, The Netherlands, and A. Lingua, P. Maschio and I. Aicardi from Politecnico di Torino, Italy, for their valuable technical support. The authors would like to also thank Dion Kant and Michel Arts for the WIPL-D simulations. This work is supported by the Netherlands Organisation for Scientific Research.

References

1. M. P. van Haarlem et al, “LOFAR: The LOw-Frequency ARray”, Astronomy & Astrophysics, vol. 556, A2, 1-53, Aug. 2013.
2. A. J. J. van Es, M. G. Labate, M. F. Waterson, J. Monari, P. Bolli, D. Davidson, R. Wayth, M. Sokolowski, P. Di Ninni, G. Pupillo, G. Macario, G. Virone, L. Ciorba, F. Paonessa, "A prototype model for evaluating SKA-LOW station calibration," Proc. SPIE 11445, Ground-based and Airborne Telescopes VIII, 1144589 (13 December 2020); https://doi.org/10.1117/12.2562391
3. P. Bolli et al., "Test-Driven Design of an Active Dual-Polarized Log-Periodic Antenna for the Square Kilometre Array," in IEEE Open Journal of Antennas and Propagation, vol. 1, pp. 253-263, 2020, doi: 10.1109/OJAP.2020.2999109.

4. I. Farhat, D. Cutajar, K. Z. Adami, C. Sammut and J. Abela, "Characterization of 36 Meter Square Mid-Frequency Radio Astronomy Prototype Antenna Array," 2018 IEEE Conference on Antenna Measurements & Applications (CAMA), Vasteras, 2018, pp. 1-3, doi: 10.1109/CAMA.2018.8530622.
5. Zhang, Y., El-Makadema, A., de Lera Acedo, E. et al. On the front-end design of mid-frequency aperture array for Square Kilometre Array. Exp. Astron., 46, 357–380 (2018). https://doi.org/10.1007/s10686-018-9608-z
6. G. W. Kant, P. D. Patel, S. J. Wijnholds, M. Ruiter, and E. van der Wal, “EMBRACE: A Multi-Beam 20,000-Element Radio Astronomical Phased Array Antenna Demonstrator,” IEEE Trans. Antennas and Prop., Vol. 59, no. 6, pp. 1990-2003, June 2011; doi: 10.1109/TAP.2011.2122233
7. Kiefner, U., Wayth, R. B., Davidson, D. B., & Sokolowski, M. (2021). Holographic calibration of phased array telescopes. Radio Science, 56, e2020RS007171. https://doi.org/10.1029/2020RS007171
8. Salas, P., Brentjens, M. A., Bordenave, D. D., Oonk, J. B. R., & Röttgering, H. J. A. (2020). Tied-array holography with LOFAR. Astronomy and Astrophysics, 635, A207. https://doi.org/10.1051/0004-6361/201935670
9. S. J. Wijnholds and W. A. van Cappellen, “In Situ Antenna Performance Evaluation of the LOFAR Phased Array Radio Telescope”, IEEE Trasn. on Antennas and Propagat., Vol. 59, No. 6, June 2011.
10. A. Nelles, et al, “Calibrating the absolute amplitude scale for air showers measured at LOFAR”, JINST 10 (2015) no.11, P11005 arXiv:1507.08932
11. E. de Lera Acedo et al., “SKA Aperture Array Verification System: Electromagnetic modeling and beam pattern measurements using a micro UAV”, Experimental Astronomy, vol. 45, issue 1, pp. 1–20, Mar. 2018. DOI: 10.1007/s10686-017-9566-x
12. P. Bolli et al., “Antenna pattern characterization of the low-frequency receptor of LOFAR by means of an UAV-mounted artificial test source,” SPIE Ground-based and Airborne Telescopes VI, Edinburgh, Scotland, United Kingdom, June 26 – July 1 2016. DOI 10.1117/12.2232419

13. G. Pupillo et al., “Medicina Array Demonstrator: calibration and radiation pattern characterization using a UAV-mounted radio-frequency source,” Experimental Astronomy, vol. 39, issue 2, pp. 405-421, June 2015. DOI: 10.1007/s10686-015-9456-z
14. P. Bolli et al., “From MAD to SAD: the Italian experience for the Low Frequency Aperture Array of SKA1-LOW”, Radio Science, vol. 51, issue 3, pp. 160–175, Mar. 2016. DOI: 10.1002/2015RS005922
15. G. Virone et al., “Strong Mutual Coupling Effects on LOFAR: Modeling and In Situ Validation,” IEEE Transactions on Antennas and Propagation, vol. 66, no. 5, pp. 2581-2588, May 2018. DOI: 10.1109/TAP.2018.2816651
16. Paonessa, F., Virone, G., Addamo, G., et al., “UAV-based pattern measurement of the SKALA”., IEEE International Symposium on Antennas and Propagation / USNC/URSI National North American Radio Science Meeting Location: Vancouver, CANADA Date: JUL 19-24, 2015
17. P. Bolli et al., “Near-Field Experimental Verification of the EM Models for the LOFAR Radio Telescope,” IEEE Antennas and Wireless Propagation Letters, vol. 17, issue 4, pp. 613–616, Apr. 2018. DOI: 10.1109/LAWP.2018.2859828
18. P. Di Ninni, P. Bolli, F. Paonessa, G. Pupillo, G. Virone, S. J. Wijnholds, “Electromagnetic Analysis and Experimental Validation of the LOFAR Radiation Patterns”, International Journal of Antennas and Propagation, January 2019, doi:10.1155/2019/9191580
19. F. Paonessa, L. Ciorba, G. Virone, P. Bolli, A. Magro, A. McPhail, D. Minchin, and R. Bhushan, “SKA-low Prototypes Deployed in Australia: Synoptic of the UAV-based Experimental Results,” Radio Science Letters, VOL. 2, 2020, DOI: 10.46620/20-0021.
20. J. Sherman, "Properties of focused apertures in the Fresnel region," in IRE Transactions on Antennas and Propagation, vol. 10, no. 4, pp. 399-408, July 1962, doi: 10.1109/TAP.1962.1137900.
21. P. Nepa and A. Buffi, "Near-Field-Focused Microwave Antennas: Near-field shaping and implementation.," in IEEE Antennas and Propagation Magazine, vol. 59, no. 3, pp. 42-53, June 2017, doi: 10.1109/MAP.2017.2686118.

22. F. Paonessa et al., “UAV-Based Antenna Measurements: Improvement of the Test Source Frequency Behavior,” 2018 IEEE Conference on Antenna Measurement and Applications (CAMA 2018), Västerås, Sweden, Sept. 3-6, 2018
23. G. Virone et al., "Preliminary Results on the Verification of the LOFAR-HBA with a Flying Test Source," 2021 15th European Conference on Antennas and Propagation (EuCAP), 2021, pp. 1-4, doi: 10.23919/EuCAP51087.2021.9411311.
24. F. Paonessa, et al. “Differential phase patterns of the LOFAR LBA array measured in situ”, 12th European Conference on Antennas and Propagation, London, UK, 9-13 April 2018
25. L. Ciorba et al., "Near-Field Phase Reconstruction for UAV-based Antenna Measurements," 2019 13th European Conference on Antennas and Propagation (EuCAP), 2019, pp. 1-4.
26. S. Pivnenko et al., "Comparison of Antenna Measurement Facilities With the DTU-ESA 12 GHz Validation Standard Antenna Within the EU Antenna Centre of Excellence," in IEEE Transactions on Antennas and Propagation, vol. 57, no. 7, pp. 1863-1878, July 2009, doi: 0.1109/TAP.2009.2021934.
27. J. L. A. Quijano and G. Vecchi, "Field and Source Equivalence in Source Reconstruction on 3D Surfaces," Progress In Electromagnetics Research, Vol. 103, 67-100, 2010. doi:10.2528/PIER10030309

Giuseppe Virone was born in Turin, Italy, in 1977. He received the degree in electronic engineering (summa cum laude) and the Ph.D. degree in electronics and communication Engineering from the Politecnico di Torino, Italy, in November 2001 and 2006, respectively. He is currently a Senior Researcher at the Istituto di Elettronica e di Ingegneria Informatica e delle Telecomunicazioni (IEIIT), Italian National Research Council (CNR). He joined IEIIT as a Research Assistant in 2002. He coordinated more than 15 scientific projects funded by both the industry and other scientific research organizations and joined more than 30 research projects as a collaborator. He authored 43 journal papers, 134 conference papers, and 3 European patents. His activities concern the design, numerical analysis, and characterization of microwave and millimeter waveguide passive components for feed systems, antenna arrays, frequency selective surfaces, compensated dielectric radomes, and industrial sensing applications.

Fabio Paonessa was born in Turin, Italy, in 1985. He received the BS and the MS degrees in biomedical engineering and the PhD degree in electronics engineering from the Polytechnic of Turin, in 2008, 2010, and 2017, respectively. From 2011 to 2012, he was a Research Assistant with the Department of Electronics, Polytechnic of Turin. In 2013, he joined the Applied Electromagnetics Group of the Institute of Electronics, Computer and Telecommunication Engineering (IEIIT), Italian National Research Council (CNR). He became Researcher in 2018. His activities include the scientific applications of the unmanned aerial vehicles for the characterization of antenna arrays and radar systems and wireless sensor networks related applications.

Lorenzo Ciorba was born in Avezzano, Italy, in 1993. He received the master's degree (110/110) in mathematical engineering from Politecnico di Torino, Italy, in March 2018, with the thesis "Hybrid Antenna Measurement and Simulations" with Prof. G. Vecchi as a supervisor. In June 2018, he joined the Applied Electromagnetics and Electronic Devices Group of the Institute of Electronics, Computer and Telecommunication Engineering (IEIIT), Italian National Research Council (CNR), as a Research Fellow. From November 2018, he has been a Ph.D. student in electrical, electronics and Communications Engineering at Politecnico di Torino. His scientific interests regard computational electromagnetics and characterization of antennas, in particular UAV-based near field antenna measurements.

Stefania Matteoli received her B.S. and M.S. (cum laude) degrees in Telecommunications Engineering and the Ph.D. in "Remote Sensing" from University of Pisa, Italy, in 2003, 2006, and

2010 respectively. She is currently a permanent researcher at the National Research Council of Italy within the Institute of Electronics, Computers and Telecommunication Engineering. From January 2010 to December 2016 she was first a post-doctoral fellow and then a temporary researcher with the Department of Information Engineering, University of Pisa, Italy. From May 2008 to October 2008, she was a visiting student at the Chester F. Carlson Center for Imaging Science, Rochester Institute of Technology, Rochester, New York. She is Associate Editor of the IEEE GEOSCIENCE AND REMOTE SENSING LETTERS and of the SPIE Journal of Applied Remote Sensing. Her main research interests include signal and image processing applied to various remote sensing applications and to antenna array data processing.

Pietro Bolli received the Laurea degree in electronic engineering and the Ph.D. degree in computer science and telecommunications engineering from the University of Florence, Italy, in 1999 and 2003, respectively. In 2002, he started his professional career as a Microwave Engineer at the Italian National Institute for Astrophysics (INAF) conducting research in the field of technology applied to radio astronomy. He is currently Senior Technologist at the INAF Arcetri Astrophysical Observatory, where he is involved in the design, characterization, and calibration of the low frequency instrument of the Square Kilometer Array. P. Bolli is the Italian responsible for the protection of the frequency bands used by radio astronomers and represents INAF in the Committee on Radio Astronomy Frequencies (CRAF). He is also Officer of the Commission J (Radio Astronomy) of the Italian Committee of the Union Radio Scientifique Internationale (URSI). He is co-author of about 140 scientific publications, which have appeared in international referred journals and conferences.

Stefan J. Wijnholds received the M.Sc. degree in astronomy and the M.Eng. degree in applied physics (both cum laude) from the University of Groningen, The Netherlands, in 2003, and the

Ph.D. degree (cum laude) from Delft University of Technology, Delft, The Netherlands, in 2010. After his graduation in 2003, he joined the R&D Department of ASTRON, the Netherlands Institute for Radio Astronomy, Dwingeloo, The Netherlands, where he works on the development of the next generation of radio telescopes based on phased array technology. From 2006 to 2010, he was also affiliated with the Delft University of Technology, Delft, The Netherlands. Since 2016, he is affiliated with the Electrical and Electronic Engineering Department of the University of Stellenbosch, South Africa, as Extraordinary (Associate) Professor. In 2018, he became a Senior Researcher at ASTRON overseeing work on the institutional technology development roadmap to address the Big Data challenges posed by large phased array systems. His research interests lie in the area of array signal processing, specifically calibration and imaging, and system design of the next generation of radio telescopes.

Biographies and photographs for the other authors are not available.

Caption List

Fig. 1 The UAV after take-off is reaching the first waypoint to perform the required scan path over the LOFAR Eastern HBA array of the CS302 station. The array dimension is about 30 m.

Fig. 2 Element positions in LOFAR HBA subarray. Red and black numbers refer to tile number (0-23) and element number (0-15) inside the single tile, respectively. The black dashed curve shows an example of a UAV path (its projection to the ground) oriented along the North-West direction.

Fig. 3 Normalized E-plane radiation pattern for tiles 6-11 (left) and 12-17 (right) at 124 MHz.

Fig. 4 Normalization constants (dB) for tiles 6-17 at 124 MHz.

Fig. 5 Far field pattern (black line) and focused near field (blue line) of tiles 6-11 (left figure) and 12-17 (right figure) at 124 MHz.

Fig. 6 Far field pattern (black line) and focused near field (blue line) of tiles 12-17 at 150 MHz (left) and 180 MHz (right).

Fig. 7 Far field pattern (black line) and focused near field (blue line) of tiles 1-24 (full HBA subarray) at 124 MHz.

Fig. 8 Far field pattern (black line) and focused near field (blue line) of tiles 1-24 (full HBA subarray) at 150 MHz.

Fig. 9 Far field pattern (black line) and focused near field (blue line) of tiles 1-24 (full HBA subarray) at 180 MHz.

Fig. 10 Measured θ- (left) and φ- (right) components of the radiated pattern of tile 9 at 180 MHz (North-West polarized elements).

Fig. 11 Measured (left) an simulated (right) beam patterns for tile 9 at 180 MHz (North-West polarized elements).

Fig. 12 Measured (left) an simulated (right) beam patterns of the HBA array in Fig. 2 at 180 MHz (North-West polarized elements).

Fig. 13 E-plane radiation patterns for tiles 12-17 at 180 MHz: magnitude (left) and phase (right).

Fig. 14. E-plane radiation pattern for tiles 12-17 at 180 MHz.

Fig. 15. E-plane radiation pattern for tiles 12-17 at 124 MHz**.**